International Journal of Naval Architecture and Ocean Engineering 11 (2019) 819–827

Contents lists available at ScienceDirect

International Journal of Naval Architecture and Ocean Engineering

journal homepage: http://www.journals.elsevier.com/international-journal-of-naval-architecture-and-ocean-engineering/

Investigation of surface-piercing fixed structures with different shapes for Bragg reflection of water waves

Wei-Wei Ding [a], Zao-Jian Zou [a, b, *], Jing-Ping Wu [c], Bai-Gang Huang [a]

[a] School of Naval Architecture, Ocean and Civil Engineering, Shanghai Jiao Tong University, Shanghai, 200240, China
[b] State Key Laboratory of Ocean Engineering, Shanghai Jiao Tong University, Shanghai, 200240, China
[c] School of Transportation, Wuhan University of Technology, Wuhan, 430063, China

ARTICLE INFO

Article history:
Received 22 September 2018
Received in revised form
31 December 2018
Accepted 27 March 2019
Available online 1 April 2019

Keywords:
Surface-piercing fixed structures
Bragg reflection
Wave attenuation
Boundary element method

ABSTRACT

Bragg reflection of water waves by three kinds of surface-piercing fixed structures with rectangular, cosinoidal and triangular shapes is studied. Boundary element method is used to analyze the wave scattering by these structures based on the linear wave theory. Results of reflection and transmission coefficients are validated by comparing with those available in literature. These structures with proper configurations are proved to be effective in attenuating waves by using Bragg reflection, and the triangular structures are found to be the best choices among the structures with same width and same area. Systematic calculations are then carried out for the triangular structures by varying the number, the draft, the width, the gap and the combination of width and gap of the structures to analyze their influences on the characteristics of Bragg reflection. The results are of reference values for design of the structures to attenuate waves based on the Bragg reflection.

1. Introduction

The attenuation of water waves is an important research topic in coastal and ocean engineering. Breakwaters consisting of single or multiple structures are often constructed to protect engineering structures or sea shore from wave attack. Compared with a single structure, multiple structures used as breakwaters may enhance the effectiveness of wave attenuation under proper geometrical deployment. If multiple structures are deployed periodically, they are known as periodical structures. When incident waves impinge on periodical structures, a resonance of reflection could occur. Specifically, the primary reflection coefficient would be achieved under the condition that the wavelength of the normally incident wave is about twice the periodical length of the periodical structures, which is defined as the phenomenon of Bragg reflection.

The occurring of Bragg reflection leads to the possibility that the periodical structures could help attenuating waves effectively. Based on the Bragg reflection, Mei et al. (1988) suggested a series of sinusoidal sandbars to protect the drilling platforms in the Ekofisk of the North Sea from wave attack. Bailard et al. (1990) concluded that a number of submerged bars based on the Bragg reflection may be an appropriate shore protection method to significantly reduce the erosion. Bailard et al. (1992) found that the Bragg reflection submerged bars were capable of providing storm erosion protection along U.S. Gulf Coast and Atlantic Coast beaches. Tsai and Wen (2010) indicated that by using the mechanism of Bragg reflection, the submerged breakwaters were effective to reflect incoming waves near Mi-Tuo Coast, Taiwan.

So far, Bragg reflection of water waves by submerged structures with a number of different shapes has been widely investigated. Most researches focused on the submerged structures with one kind of shape, such as rectangular shape (Hsu et al. (2003); Wen and Tsai (2008); Zeng et al. (2017)), sinusoidal or cosinoidal shape (Cho and Lee (2000); Cho et al. (2004); Shih and Weng (2016)), trapezoidal shape (Jeon and Cho (2006); Chang and Liou (2007)), parabolic shape (Liu et al. (2015)) and semi-circular shape (Liu et al. (2016)). Several kinds of shapes were also considered simultaneously. Hsu et al. (2002) experimentally and theoretically analyzed the characteristics of Bragg reflection of water waves by three kinds of submerged artificial bars with rectangular, triangular and rectified cosinoidal shapes, respectively. Tsai et al. (2011) proposed multiply composite artificial bars with

* Corresponding author. School of Naval Architecture, Ocean and Civil Engineering, Shanghai Jiao Tong University, 800 Dongchuan Road, Shanghai, 200240, China.
E-mail address: zjzou@sjtu.edu.cn (Z.-J. Zou).
Peer review under responsibility of Society of Naval Architects of Korea.

https://doi.org/10.1016/j.ijnaoe.2019.03.006

different shapes, such as rectangular, triangular and rectified sinusoidal, in which two kinds of periodical length were considered. The effective bandwidth of Bragg reflection could be enlarged by these bars. Liu et al. (2014) analytically investigated the Bragg reflection of long waves by three kinds of submerged bars with triangular shape, rectified cosinoidal shape, and idealized trapezoidal shape, respectively. Optimal curves for the maximum Bragg resonance were obtained to help designing these Bragg breakwaters.

Above researches mainly focused on the Bragg reflection of water waves by submerged structures on the seabed. However, these structures can also be arranged piercing the still water surface or under the still water surface. According to the physical essence of the occurring of Bragg reflection, these structures enduring incident water waves may also induce the phenomenon of Bragg reflection. Garnaud and Mei (2010) investigated the wave scattering and radiation by an array of small heaving buoys that were attached to power-takeoff devices based on an asymptotic theory. It was found that the phenomenon of Bragg reflection significantly reduced the extraction efficiency of wave energy. Linton (2011) studied the scattering of water waves over periodical arrays of submerged horizontal circular cylinders in deep water using the multiple expansion technique. A phase shift in the phenomenon of Bragg reflection was found compared with the standard Bragg law. Karmakar et al. (2013) analyzed the wave scattering by multiple vertical flexible membranes using the eigenfunction expansion method, and found the phenomenon of Bragg reflection in the wave interaction with two vertical flexible membranes. Ouyang et al. (2015) investigated the Bragg reflection of water waves by a series of stationary floating pontoon breakwaters with rectangular shape based on a boundary discretization technique. Ding et al. (2018) proposed the multiple composite flexible membranes floating vertically in the water and found that the effective bandwidth of Bragg reflection could be increased compared with the traditional multiple flexible membranes.

In the researches above, a number of methods have been utilized in the problem of wave interaction with structures. Meanwhile, the boundary element method is also widely used in the wave interaction with structures, especially for the complex engineering structures (Teng and Gou (2017)). For example, Dalrymple and Kirby (1986) proved that the boundary element method was accurate and effective to investigate the interaction between water waves and a patch of bottom ripples. Kar et al. (2018) used the boundary element method to analyze the surface gravity wave scattering by a pair of trenches. The boundary element method is quite convenient to deal with complex geometries of structures. Moreover, many kinds of structures with different shapes can be easily considered by the boundary element method.

There are only few researches on the Bragg reflection of water waves arising from surface-piercing fixed structures with different shapes. In this paper, three surface-piercing fixed structures with rectangular, cosinoidal and triangular shapes are chosen as typical examples for the study of Bragg reflection of water waves. Structures with these three shapes are reasonable choices from the engineering point of view and were analyzed by Hsu et al. (2002) and Tsai et al. (2011) for the cases of structures fixed on the seabed. The present study extends the work of Ouyang et al. (2015) in which only the fixed floating pontoon with rectangular shape was considered. Meanwhile, the boundary element method is adopted to conveniently consider the structures with different shapes. Numerical solutions based on the boundary element method are derived and validated with published results in the literature. The differences in Bragg reflection induced by the three kinds of structures with rectangular, cosinoidal and triangular shapes are analyzed. Characteristics of Bragg reflection are systematically investigated with the variation of the number, the draft and the width, the gap and the combination of width and gap of the triangular structures. This study can provide guidance on design of surface-piercing fixed structures with different shapes to attenuate waves when taking advantage of Bragg reflection.

2. Mathematical formulation

As shown in Fig. 1, three kinds of surface-piercing fixed structures deployed on the still water surface are considered. Each kind of the structures consists of same structures, whose shapes under the still water surface are rectangular, cosinoidal and triangular respectively, with the width W and the draft d. The number of the structures is N. The gap between every two adjacent structures keeps the same and is denoted by S. These structures can then be seen as periodical structures with the periodical length $L = S + W$.

A monochromatic incident wave with frequency ω and small amplitude a_m approaches the structures from the far field. The wave scattering problem of the structures is analyzed based on the linear water wave theory in which the fluid is assumed to be inviscid and incompressible and the flow is assumed to be irrotational. The seabed is assumed to be uniform and impermeable. The water depth keeps constant and is denoted by h.

A two dimensional Cartesian coordinate system is defined, with x-axis pointing horizontally right and z-axis pointing vertically upward. The origin is set at the still water surface and the center of the first structure for mathematical convenience.

Under the frame of linear potential theory, the flow in the whole region can be described by a velocity potential $\Phi(x,z,t)$, where t is the time. For the problem considered here, the velocity potential can be expressed as

$$\Phi(x,z,t) = \mathrm{Re}\left\{\phi(x,z)e^{-i\omega t}\right\} \tag{1}$$

where Re represents the real part of the quantity, $\phi(x,z)$ is the spatial velocity potential and i represents the imaginary unit.

The velocity potential of the aforementioned incident wave can be expressed as

$$\phi_I = -\frac{ia_m g}{\omega}e^{ikx}\frac{\cosh k(h+z)}{\cosh kh} \tag{2}$$

where g is the gravitational acceleration and k is the wave number of the incident wave, which is the positive root of the dispersion equation $\omega^2 = gk\tanh kh$.

The fluid motion is governed by the two-dimensional Laplace equation

$$\left(\frac{\partial^2}{\partial x^2} + \frac{\partial^2}{\partial z^2}\right)\phi = 0 \tag{3}$$

By combining the linearized kinematic and dynamic free surface boundary conditions, the linearized free surface boundary condition is obtained as

$$\frac{\partial\phi}{\partial z} - \frac{\omega^2}{g}\phi = 0 \quad , \qquad z = 0 \tag{4}$$

The fixed structures are assumed to be rigid. The boundary condition on the surface of each structure can be expressed as

$$\nabla\phi\cdot\boldsymbol{n} = 0 \tag{5}$$

where $\boldsymbol{n}$ represents the unit normal vector.

The impermeable seabed condition is

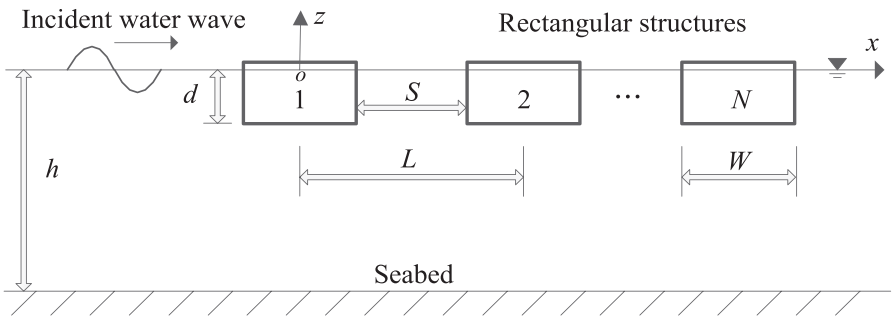

a) Rectangular structures

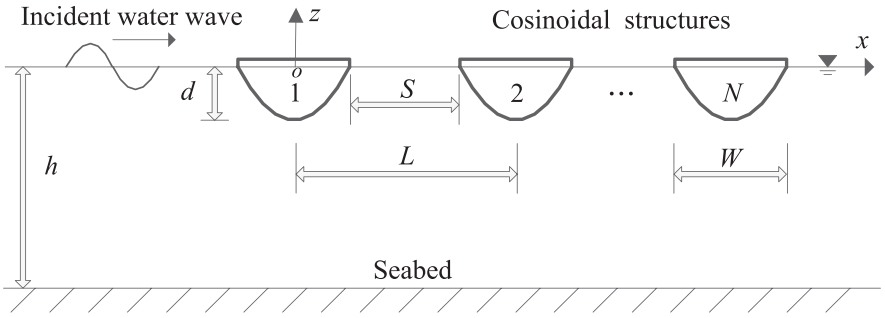

b) Cosinoidal structures

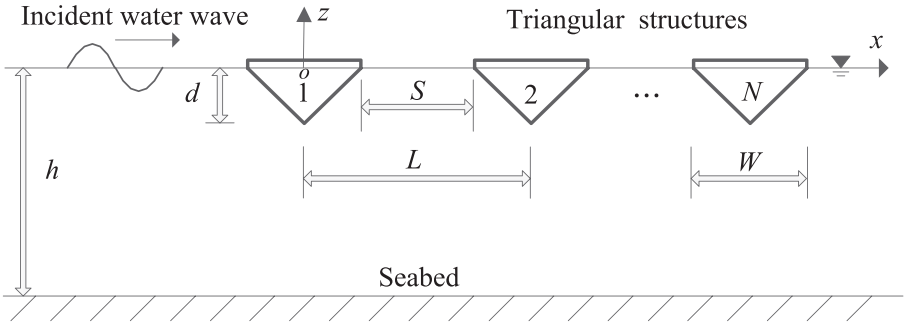

c) Triangular structures

Fig. 1. Sketch map of the surface-piercing fixed structures with different shapes.

$$\frac{\partial \phi}{\partial z} = 0 \ , \qquad z = -h. \tag{6}$$

The Sommerfeld boundary conditions are given as

$$\lim_{x \to \mp\infty} \left(\frac{\partial}{\partial x} \pm ik \right) \begin{pmatrix} \phi - \phi_{\mathrm{I}} \\ \phi \end{pmatrix} = 0 \tag{7}$$

3. Numerical solutions

The boundary element method is used to solve the boundary value problem formulated above. Two hypothetic boundaries at $x = x_l$ and $x = x_r$ respectively are introduced to facilitate the numerical solutions, where x_l is located sufficiently far from the first structure, and x_r is located sufficiently far from the last structure. Accordingly, the whole region is divided into the region 1 ($x \le x_l$), the region 2 ($x_l < x < x_r$) and the region 3 ($x \ge x_r$), and the velocity potentials in the three regions are represented by $\phi_1(x,z)$, $\phi_2(x,z)$ and $\phi_3(x,z)$, respectively.

The velocity potential in the region 1, which fulfills Eq. (7), can be expressed as

$$\phi_1(x,z) = \left[A_{\mathrm{I}} e^{ik(x-x_l)} + R e^{-ik(x-x_l)} \right] \frac{\cosh k(h+z)}{\cosh kh}, \qquad A_{\mathrm{I}} = -\frac{i a_m g}{\omega} e^{ikx_l} \tag{8}$$

where R is the complex amplitude of the reflection coefficient and A_{I} is introduced for expression convenience.

The velocity potential in the region 3, which fulfills Eq. (7), can be expressed as

$$\phi_3(x,z) = Te^{ik(x-x_r)}\frac{\cosh k(h+z)}{\cosh kh} \tag{9}$$

where T is the complex amplitude of the transmission coefficient.

According to the continuity of pressure and the continuity of velocity at the two hypothetic boundaries, it has

$$\phi_2(x,z)|_{x=x_l} = \phi_1(x,z)|_{x=x_l} \tag{10}$$

$$\left.\frac{\partial\phi_2(x,z)}{\partial x}\right|_{x=x_l} = \left.\frac{\partial\phi_1(x,z)}{\partial x}\right|_{x=x_l} \tag{11}$$

$$\phi_2(x,z)|_{x=x_r} = \phi_3(x,z)|_{x=x_r} \tag{12}$$

$$\left.\frac{\partial\phi_2(x,z)}{\partial x}\right|_{x=x_r} = \left.\frac{\partial\phi_3(x,z)}{\partial x}\right|_{x=x_r} \tag{13}$$

By substituting Eq. (8) into the combination of Eq. (10) and Eq. (11), the boundary condition at $x = x_l$ can be derived as

$$\left[\phi_2 + \frac{1}{ik}\frac{\partial\phi_2}{\partial x}\right]_{x=x_l} = 2A_I\frac{\cosh k(h+z)}{\cosh kh} \tag{14}$$

By substituting Eq. (9) into the combination of Eq. (12) and Eq. (13), the boundary condition at $x = x_r$ can be derived as

$$\left[\phi_2 - \frac{1}{ik}\frac{\partial\phi_2}{\partial x}\right]_{x=x_r} = 0 \tag{15}$$

The free surface Green function, which is the fundamental solution to Laplace Eq. (3), is defined as

$$G(P,Q) = -\ln r(P,Q) = -\frac{1}{2}\ln\left[(x-\xi)^2 + (z-\eta)^2\right] \tag{16}$$

where $P(x,z)$ is the field point, $Q(\xi,\eta)$ is the source point, and $r = \sqrt{(x-\xi)^2+(z-\eta)^2}$ represents the distance between the field point and the source point.

This kind of Green function is simple and the phenomenon of irregular frequencies due to numerical discretization is unlikely to occur. By using Green's theorem, the velocity potential at point P located in the region 2 (excluding its boundaries) fulfills the relation

$$-2\pi\phi_2(P) = \oint_C\left(\phi_2(Q)\frac{\partial G(P,Q)}{\partial n} - G(P,Q)\frac{\partial\phi_2(Q)}{\partial n}\right)ds \tag{17}$$

where the direction of definite integration is anticlockwise; the total boundary C consists of the hypothetic left boundary C_l, the seabed boundary C_s, the hypothetic right boundary C_r, several still water surface boundaries C_w and several structure surface boundaries C_b.

Based on Eq. (17), the velocity potential at any location in the region can be represented in terms of the values of the velocity potential and its normal derivative on the boundaries. When the point P is located on the boundaries of the region 2, Eq. (17) is rewritten as

$$-\pi\phi_2(P) = \oint_C\left(\phi_2(Q)\frac{\partial G(P,Q)}{\partial n} - G(P,Q)\frac{\partial\phi_2(Q)}{\partial n}\right)ds \tag{18}$$

In order to numerically obtain the velocity potential on the total boundaries, all the boundaries are divided into a number of small elements. The sharp corner of the boundaries of the structures is set as the endpoints of the adjacent elements. The constant element model is adopted, and a constant velocity potential exists on each element. The collocation point and the source point are set at the midpoint of each element. Although there are more sophisticated element models, the accuracy of results is about the same as long as a sufficient number of elements in the constant element model are used.

By substituting Eqs. (4)–(6), (14) and (15) into Eq. (18) and discreting the resulting equation, it gives

$$\begin{aligned}&\pi\phi_2^e(P) + \sum_{C_w}\left(h^{PQ} - \frac{\omega^2}{g}g^{PQ}\right)\phi_2^e(Q) + \sum_{C_b+C_s}h^{PQ}\phi_2^e(Q) + \sum_{C_l+C_r}\left(h^{PQ}\right.\\ &\left.- ikg^{PQ}\right)\phi_2^e(Q)\\ &= \sum_{C_l}2ikA_I\frac{\cosh k(h+z)}{\cosh kh}g^{PQ}\end{aligned} \tag{19}$$

where $h^{PQ} = \int_{\Gamma_Q}\frac{\partial G(P,Q)}{\partial n}d\Gamma$ and $g^{PQ} = \int_{\Gamma_Q}G(P,Q)d\Gamma$, which are introduced for expression convenience; ϕ_2^e represents the velocity potential on the element e.

The values of h^{PQ} and g^{PQ} can be calculated numerically via common Gaussian quadrature. Particularly, when the point Q and the point P overlap, the singularity of Green function occurs and the values of h^{PQ} and g^{PQ} are explicitly obtained as

$$h^{PQ} = 0 \tag{20}$$

$$g^{PQ} = \frac{\Delta l}{2\pi}\left(1 + \ln\frac{2}{\Delta l}\right) \tag{21}$$

where Δl represents the length of the element on which Q locates.

Denoting the total number of the elements as M, M linear algebraic equations similar to Eq. (19) can be established. The velocity potential on each element can then be determined by solving these equations.

By substituting Eq. (8) into Eq. (10) and multiplying both sides of the resulting equation with $\cosh k(h+z)$, it gives

$$\phi_2(x_l,z)\cosh k(h+z) = (A_I + R)\frac{\cosh^2 k(h+z)}{\cosh kh} \tag{22}$$

Integrating Eq. (22) with respect to z from -h to 0, it follows

$$R = -A_I + \frac{k}{n_0\sinh kh}\int_{-h}^{0}\phi_2(x_l,z)\cosh k(h+z)dz \tag{23}$$

where $n_0 = \frac{1}{2}\left(1 + \frac{2kh}{\sinh kh}\right)$.

By substituting Eq. (9) into Eq. (12) and multiplying both sides of the resulting equation with $\cosh k(h+z)$, it gives

$$\phi_2(x_r,z)\cosh k(h+z) = T\frac{\cosh^2 k(h+z)}{\cosh kh} \tag{24}$$

Integrating Eq. (24) with respect to z from -h to 0, it follows

$$T = \frac{k}{n_0\sinh kh}\int_{-h}^{0}\phi_2(x_r,z)\cosh k(h+z)dz \tag{25}$$

Thus, the reflection and transmission coefficients can be

calculated as

$$Kr = |R/A_I| \tag{26}$$

$$Kt = |T/A_I| \tag{27}$$

4. Results and discussion

The purpose of the present study is to analyze the effectiveness of wave attenuation through the Bragg reflection induced by the surface-piercing fixed structures with various shapes. Three parameters, namely the occurring condition, the primary reflection coefficient and the effective bandwidth, are adopted to represent the characteristics of Bragg reflection. The occurring condition is defined by the value of $2L/\lambda$ when the phenomenon of Bragg reflection occurs, where λ is the wave length. The primary reflection coefficient Kp is the corresponding peak reflection coefficient when the phenomenon of Bragg reflection occurs. The effective bandwidth E_b is defined as the range of the value of $2L/\lambda$ in the region of Bragg reflection under the condition $Kr \geq Kp/2$. Well-designed surface-piercing fixed structures based on Bragg reflection are expected to be capable of effectively reflecting waves in a wide range of wave frequencies. The primary reflection coefficient and the effective bandwidth are of importance in engineering design.

4.1. Validation of the method

The distance between the hypothetic boundary and its adjacent structure is set as four times of the water depth, which is far enough to ignore the effects of evanescent waves according to Ding et al. (2018). According to Liu and Abbaspour (1982), about eight small elements within a wavelength are needed in using the boundary element method. In the present study, a smaller mesh size is selected and the minimum number of small elements within a wavelength is 25. The mesh size on the body surface is about the same as that on the free surface. Numerical results using these settings show that the convergence of the reflection and transmission coefficients can be achieved, and the error of the energy conservation equation $Kr^2 + Kt^2 = 1.0$ is less than 0.2%.

Ouyang et al. (2015) introduced a Radial Basis Function (different from the present Green Function) to satisfy the Laplace equation and further developed a numerical model of boundary discretization type to investigate the wave scattering by rectangular structures. Fig. 2 shows the comparisons of the reflection and transmission coefficients of the structures with $N = 1$, $d/h = 0.25$ and $W/h = 0.5$ obtained by the present study and by Ouyang et al. (2015). Fig. 3 shows the comparisons of the reflection coefficient of the structures with $N = 3$, $d/h = 0.25$, $W/h = 0.5$ and $S/h = 2.0$. Excellent agreements can be observed, which demonstrates the validity of the present boundary element method.

4.2. Advantage of Bragg reflection

Take the structures with rectangular shape as an example for the analysis on the advantage of Bragg reflection. Bragg reflection of water waves by submerged structures on the seabed has been widely investigated in previous studies. When the same structures are deployed on the water surface as surface-piercing fixed structures, the phenomenon of Bragg reflection may be different. Fig. 4 shows the comparisons of the reflection coefficient of the surface-piercing fixed structures and the submerged structures on the seabed under the same geometric parameters $N = 3$, $d/h = 0.25$, $W/h = 0.5$ and $S/h = 2.5$. The phenomenon of Bragg

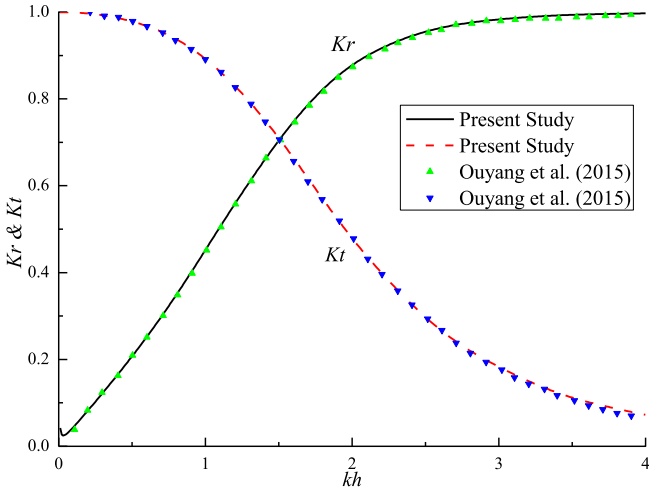

Fig. 2. Comparisons of the reflection and transmission coefficients of the structures. $N = 1$, $d/h = 0.25$ and $W/h = 0.5$

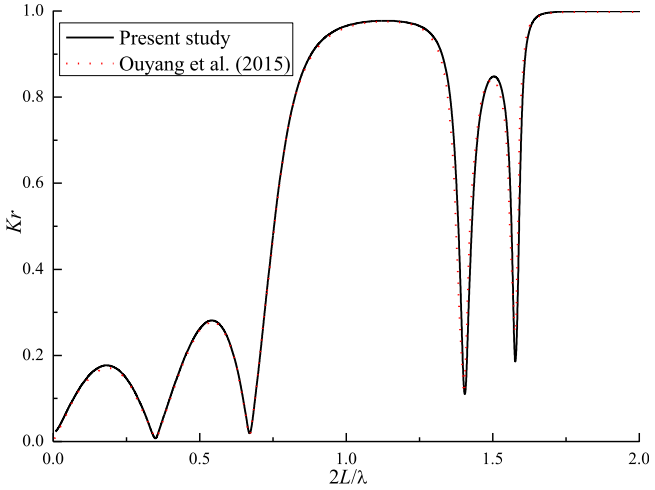

Fig. 3. Comparisons of the reflection coefficient of the structures. $N = 3$, $d/h = 0.25$, $W/h = 0.5$ and $S/h = 2.0$

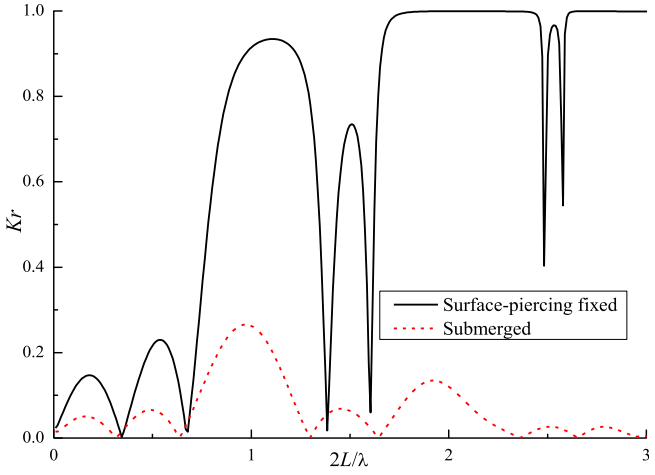

Fig. 4. Comparisons of the reflection coefficient of the surface-piercing fixed structures and the submerged structures on the seabed with $N = 3$, $d/h = 0.25$, $W/h = 0.5$ and $S/h = 2.5$

reflection can be obviously observed for both kinds of structures. However, both the primary reflection coefficient and the effective bandwidth of the surface-piercing fixed structures are much larger than those of the submerged structures on the seabed. According to the linear wave theory, the wave energy rapidly decreases from the water surface to the seabed. This may help explaining the above difference of primary reflection coefficient. As it is known, the primary reflection coefficient can be enlarged by increasing the number of submerged structures on the seabed. From Fig. 4, it can be deduced that to obtain the same primary reflection coefficient, the number of the surface-piercing fixed structures is smaller compared with the submerged structures on the seabed. Therefore, when taking advantage of Bragg reflection induced by periodical structures to attenuate waves, it may be a better choice to adopt surface-piercing fixed structures.

For surface-piercing fixed structures, three cases, i.e., (a) $N = 3$, $W/h = 0.5$ and $S/h = 2.5$, (b) $N = 1$ and $W/h = 1.5$, and (c) $N = 1$ and $W/h = 0.5$, are considered to further analyze the advantage of Bragg reflection. In all these cases, $d/h = 0.25$. Fig. 5 shows the reflection coefficient of the structures versus the nondimensional wavenumber for these cases.

For case (a), the phenomenon of Bragg reflection can be observed. The primary reflection coefficient $Kp = 0.93$ at $kh = 1.16$. The corresponding occurring condition of Bragg reflection is $2L/\lambda = 1.11$, which is in the vicinity of the traditional occurring condition $2L/\lambda = 1.0$. For case (b) and case (c), the reflection coefficient keeps increasing as the nondimensional wavenumber increases. The former always has the larger reflection coefficient due to the larger width of the single structure. It can be seen that the single structure has the better wave attenuation efficiency in most of the wavenumber range. However, in the region where the Bragg reflection occurs, the structures in case (a) have a significant advantage over the single structure in case (b) and case (c) to attenuate waves. The reflection coefficients at $kh = 1.16$ in case (b) and case (c) are $Kr = 0.84$ and $Kr = 0.54$, respectively. They are obviously smaller than the primary reflection coefficient $Kp = 0.93$ in case (a), although the width of the single structure in case (b) is the same as the equivalent width of the structures in case (a). Thus, the Bragg reflection induced by the surface-piercing fixed structures with proper configurations indeed has application value in attenuating waves.

4.3. Comparisons of the structures with different shapes

As shown in Fig. 1, three kinds of surface-piercing fixed structures with different shapes, namely rectangular, cosinoidal and triangular, are considered. The area of the single rectangular structure is $A_1 = d \times W$, the area of the single cosinoidal structure is $A_2 = 2 \times d \times W/\pi$, and the area of the single triangular structure is $A_3 = d \times W/2$. Fig. 6 shows the comparisons of the reflection coefficient of the three kinds of structures with the same geometric parameters $N = 3$, $d/h = 0.25$, $W/h = 0.5$ and $S/h = 2.5$. It can be seen that the rectangular structures have the largest primary reflection coefficient, while the triangular structures have the smallest primary reflection coefficient, which are consistent with the area of the structures. This is because that with the same draft and same width, the area of the structures plays an important role in attenuating waves, and the larger area provides the larger volume for wave reflection. The occurring condition and the effective bandwidth of the cosinoidal structures and the triangular structures are almost the same, because the difference in their areas is small. However, the occurring condition of the rectangular structures moves to left slightly. This may be due to its much larger area compared with those of other two structures. Similar results were found in Hsu et al. (2002), though the structures were fixed on the seabed in their study.

Engineering cost is closely related to the amount of construction material. For the structures considered here, same areas of the structures means the same amount of construction material. To see which kind of structures with same areas is the most efficient one, the three structures with same areas and same widths but different shapes are analyzed. The drafts of the rectangular, cosinoidal and triangular structures are denoted by d_1, d_2 and d_3, respectively. Setting $d_1/h = 0.25$ for the rectangular structures, it requires that $d_2 = \pi \times d_1/2$ for the cosinoidal structures and $d_3 = 2d_1$ for the triangular structures. Comparisons of the reflection coefficient of the three kinds of structures with $N = 3$, $W/h = 0.5$ and $S/h = 2.5$ are shown in Fig. 7. It can be seen that the occurring conditions of Bragg reflection of the three kinds of structures are almost the same, indicating that the shape of the structures has few effects on the wavelength corresponding to the Bragg reflection. However, the triangular structures have the largest primary reflection coefficient and the largest effective bandwidth, while the rectangular structures have the smallest primary reflection coefficient and the smallest effective bandwidth. This is probably due to the largest

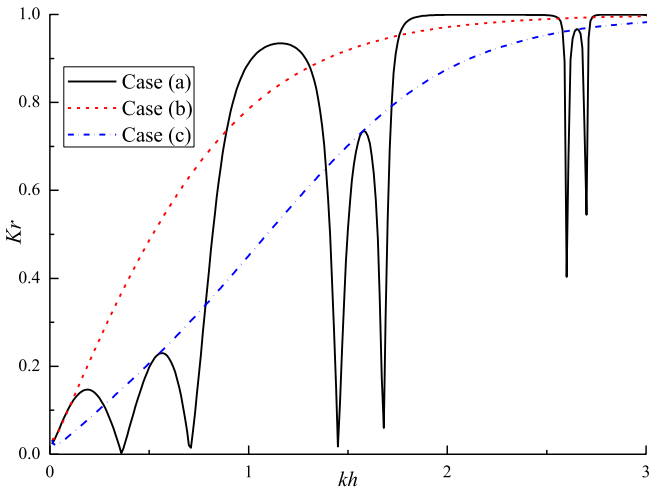

Fig. 5. Comparisons of the reflection coefficient of the structures, $d/h = 0.25$ for case (a) $N = 3$, $W/h = 0.5$ and $S/h = 2.5$; case (b) $N = 1$ and $W/h = 1.5$; and case (c) $N = 1$ and $W/h = 0.5$

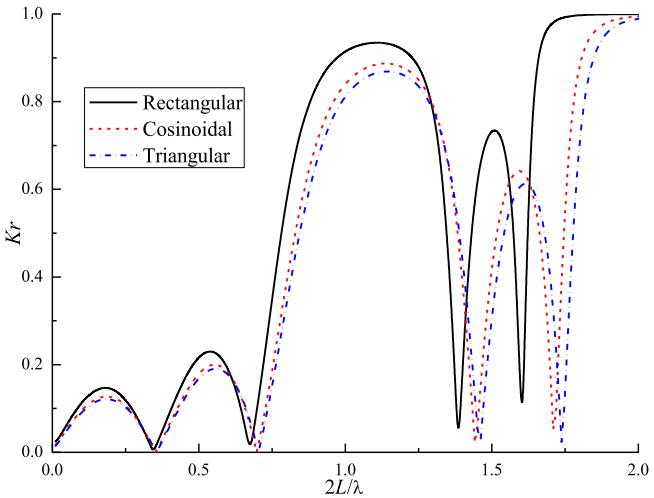

Fig. 6. Comparisons of the reflection coefficient of the three kinds of structures. $N = 3$, $d/h = 0.25$, $W/h = 0.5$ and $S/h = 2.5$

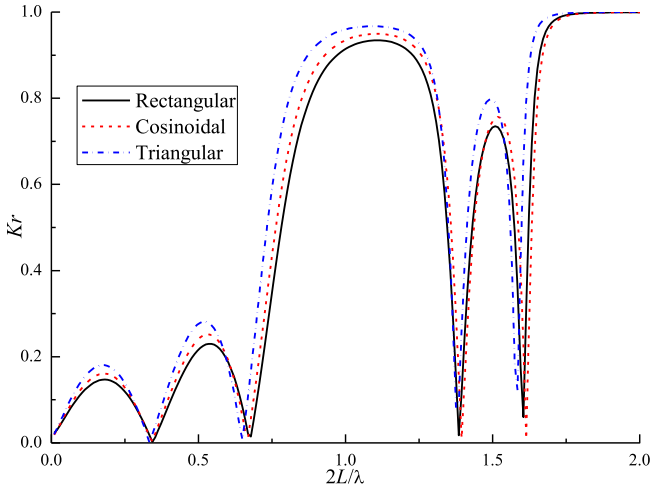

Fig. 7. Comparisons of the reflection coefficient of the three kinds of structures of same areas. $N = 3$, $W/h = 0.5$ and $S/h = 2.5$

draft of the triangular structures, and the larger draft can reflect more waves back. The larger the primary reflection coefficient and the effective bandwidth, the more beneficial to take advantage of Bragg reflection. Therefore, from both aspects of effectiveness of wave attenuation and material cost, the triangular structures may be the best choices in practical engineering.

In the following analysis on the characteristics of Bragg reflection, surface-piercing fixed structures with triangular shape are chosen. A series of parametric studies are conducted to investigate the effects of the number, the draft, the width, the gap and the combination of width and gap of the structures.

4.4. Effects of the number of the structures

Fig. 8 shows the reflection coefficient Kr versus $2L/\lambda$ for different numbers of the structures with $d/h = 0.25$, $W/h = 0.5$ and $S/h = 2.5$. Table 1 summarizes the characteristics of Bragg reflection. It can be seen that the variation of the reflection coefficient is rather complicated, with several crests and valleys in the whole range of $2L/\lambda$. For the structures with larger number, more crests and valleys of the reflection coefficient can be observed. The phenomenon of

Table 1
Characteristics of Bragg reflection of the structures with different numbers. $d/h = 0.25$, $W/h = 0.5$ and $S/h = 2.5$

N	2L/λ	Kp	E_b
3	1.15	0.87	0.83–1.39
4	1.13	0.94	0.86–1.34
5	1.11	0.97	1.11–1.31

Bragg reflection can be apparently observed for all the structures with different numbers. Meanwhile, all the occurring conditions of Bragg reflection are in the vicinity of $2L/\lambda = 1.0$. The occurring condition has a slight shift towards left with the increase of the number of the structures, indicating that the wavelength corresponding to the Bragg reflection becomes larger. When the number of the structures increases, the primary reflection coefficient keeps increasing, and nearly total reflection can be achieved finally. For example, $Kp = 0.97$ at $N = 5$. Such a large reflection coefficient is very favorable for the structures to attenuate waves effectively. However, the corresponding effective bandwidth becomes narrower and the engineering cost becomes higher for the larger number of the structures. In practical design, the number of the structures should be carefully chosen according to the required primary reflection coefficient and the effective bandwidth.

4.5. Effects of the draft of the structures

Fig. 9 shows the reflection coefficient Kr versus $2L/\lambda$ for different drafts of the structures with $N = 3$, $W/h = 0.5$ and $S/h = 2.5$. Table 2 summarizes the characteristics of Bragg reflection. Similar variation tendency of the reflection coefficient can be observed for all the drafts. All the occurring conditions of Bragg reflection are in the vicinity of $2L/\lambda = 1.0$. Moreover, the occurring condition gradually moves to left as the draft of the structures increases. The primary reflection coefficient increases as the draft of the structures becomes larger. It is apparently because more waves can be obstructed by the structures with larger draft. The effective bandwidth moves to left as a whole and at the same time becomes wider with the increasing draft of the structures. For practical applications, the structures with larger draft would be more advisable, because not only the higher reflection coefficient can be achieved, but also the wider applicable effective bandwidth is realized.

According to the traditional occurring condition of Bragg

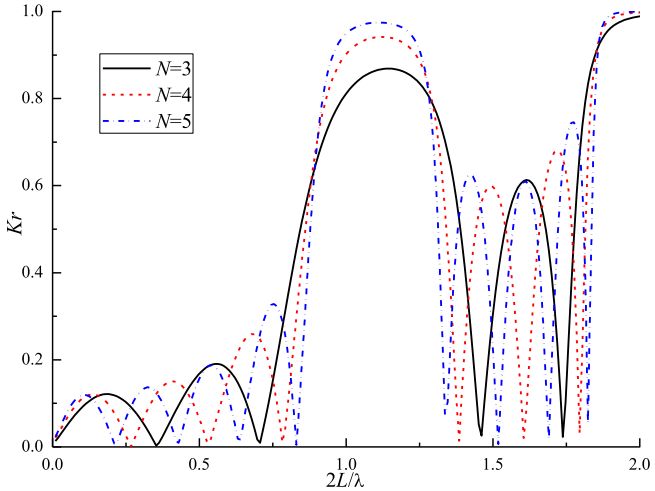

Fig. 8. Reflection coefficient versus $2L/\lambda$ with respect to the number of the structures. $d/h = 0.25$, $W/h = 0.5$ and $S/h = 2.5$

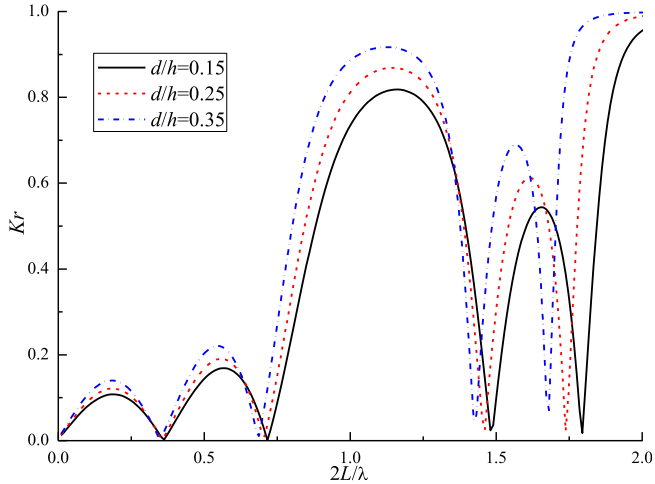

Fig. 9. Reflection coefficient versus $2L/\lambda$ with respect to the draft of the structures. $N = 3$, $W/h = 0.5$ and $S/h = 2.5$

Table 2
Characteristics of Bragg reflection of the structures with different drafts. $N = 3$, $W/h = 0.5$ and $S/h = 2.5$

d/h	2L/λ	Kp	E_b
0.15	1.16	0.82	0.86–1.41
0.25	1.15	0.87	0.83–1.39
0.35	1.13	0.92	0.79–1.38

Table 3
Characteristics of Bragg reflection of the structures with different widths. $N = 3$, $d/h = 0.25$ and $S/h = 2.5$

W/h	2L/λ	Kp	E_b
0.3	1.10	0.76	0.83–1.31
0.5	1.15	0.87	0.83–1.39
0.7	1.19	0.93	0.84–1.48

reflection $2L/\lambda = 1.0$, the phenomenon of Bragg reflection is strongly associated with the periodical length of the structures when the wavelength of incident wave is constant. The periodical length of the surface-piercing fixed structures is $L = S + W$. There exist three kinds of situations: First, the gap S of the structures is fixed, the width W of the structures varies, and thus the periodical length L of the structures varies. Second, the width W of the structures is fixed, the gap S of the structures varies, and thus the periodical length L of the structures varies. Third, the periodical length L of the structures is fixed, and both the gap S and the width W of the structures vary. In the following, the effects of the three kinds of situations on the characteristics of Bragg reflection are analyzed respectively.

4.6. Effects of the width of the structures

Fig. 10 shows the reflection coefficient Kr versus $2L/\lambda$ for different widths of the structures with $N = 3$, $d/h = 0.25$ and $S/h = 2.5$. Table 3 summarizes the characteristics of Bragg reflection. The occurring condition of Bragg reflection significantly moves to right as the width of the structures increases. For example, the occurring condition at $W/h = 0.3$ is $2L/\lambda = 1.10$, and the occurring condition at $W/h = 0.7$ becomes $2L/\lambda = 1.19$. The former is still in the vicinity of the traditional occurring condition $2L/\lambda = 1.0$, while the latter has an obvious deviation. As the width of the structures becomes larger, both the primary reflection coefficient and the effective bandwidth increase significantly. For the structures with larger width, more wave energy can be reflected in a wider range of wavelength, especially for the waves of larger wavelength. However, the structures with too larger width can be replaced by several structures with smaller width, which can utilize the induced Bragg reflection to help attenuating waves, as analyzed in subsection 4.2.

4.7. Effects of the gap of the structures

Fig. 11 shows the reflection coefficient Kr versus $2L/\lambda$ for different gaps of the structures with $N = 3$, $d/h = 0.25$ and $W/h = 0.5$. Table 4 summarizes the characteristics of Bragg reflection. As the gap of the structures increases, the occurring condition of Bragg reflection continually moves to left, and becomes closer to the traditional occurring condition of Bragg reflection $2L/\lambda = 1.0$. For example, the occurring condition at $S/h = 1.5$ is $2L/\lambda = 1.25$, at $S/h = 3.5$ is $2L/\lambda = 1.11$. The latter can be regarded as still in the vicinity of the traditional occurring condition $2L/\lambda = 1.0$, while the former has an obvious deviation. The primary reflection coefficient has an obvious increase and the effective bandwidth becomes wider with the deceasing gap of the structures. However, the wavelength corresponding to the primary reflection coefficient is much smaller at $S/h = 1.5$, compared with that at $S/h = 3.5$. Thus, the use of the structures with small gap is limited to attenuating waves with short wavelength. In practice, the gap of the structures may be adjusted according to the actual wavelength of incident wave to obtain the required effectiveness of wave attenuation.

4.8. Effects of the combination of width and gap of the structures

Fig. 12 shows the reflection coefficient Kr versus $2L/\lambda$ for different combinations of width and gap of the structures with $N = 3$, $d/h = 0.25$ and $L/h = 3.0$. Table 5 summarizes the characteristics of Bragg reflection. The effects of the combination of width and gap of the structures on the characteristics of Bragg reflection can be found to be consistent with the findings in the above subsections. For example, the primary reflection coefficient can be enlarged by increasing the width of the structures and decreasing the gap of the structures.

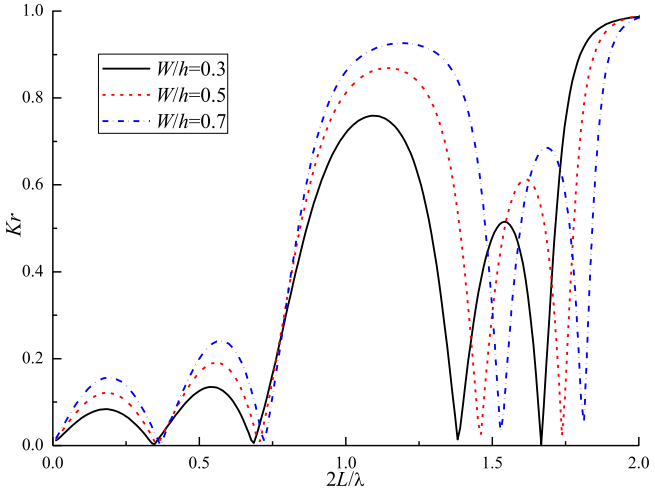

Fig. 10. Reflection coefficient versus $2L/\lambda$ with respect to the width of the structures. $N = 3$, $d/h = 0.25$ and $S/h = 2.5$

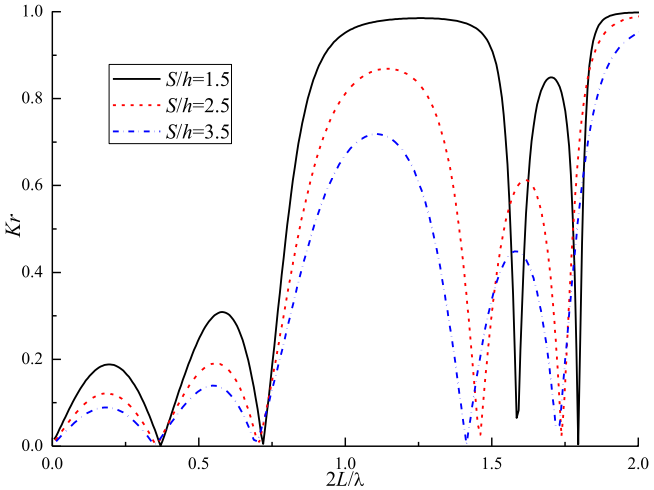

Fig. 11. Reflection coefficient versus $2L/\lambda$ with respect to the gap of the structures. $N = 3$, $d/h = 0.25$ and $W/h = 0.5$

Table 4
Characteristics of Bragg reflection of the structures with different gaps. $N = 3$, $d/h = 0.25$ and $W/h = 0.5$

S/h	2L/λ	Kp	E_b
1.5	1.25	0.99	0.80–1.56
2.5	1.15	0.87	0.83–1.39
3.5	1.11	0.72	0.84–1.34

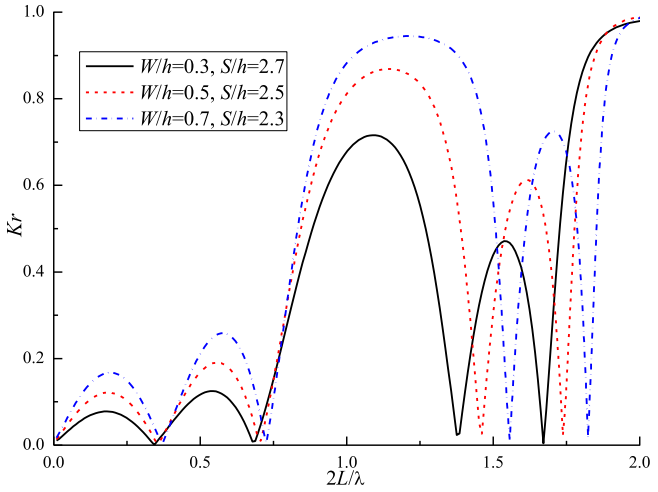

Fig. 12. Reflection coefficient versus $2L/\lambda$ with respect to the combination of width and gap of the structures. $N = 3$, $d/h = 0.25$ and $L/h = 3.0$

Table 5
Characteristics of Bragg reflection of the structures with different combinations of width and gap. $N = 3$, $d/h = 0.25$ and $L/h = 3.0$

W/h	S/h	2L/λ	Kp	E_b
0.3	2.7	1.09	0.72	0.83–1.31
0.5	2.5	1.15	0.87	0.83–1.39
0.7	2.3	1.21	0.94	0.83–1.51

5. Conclusions

Bragg reflection of water waves by surface-piercing fixed structures with three kinds of shapes, namely rectangular, cosinoidal and triangular, is investigated. The boundary element method is used to solve the problem of wave scattering by these structures based on the linear wave theory. The calculated reflection and transmission coefficients are compared with results available in the literature to verify the validity and accuracy of the method.

It is concluded that the surface-piercing fixed structures with proper configurations can effectively attenuate waves when making use of Bragg reflection, and among the three kinds of structures with same width and same area, the triangular structures are the best choice from overall consideration. Then the characteristics of Bragg reflection are systematically analyzed for the triangular structures by changing the number, the draft, the width, the gap and the combination of width and gap of the structures. The occurring condition in most situations is in the vicinity of traditional occurring condition of Bragg reflection. The primary reflection coefficient can be enlarged by increasing the number and the draft of the structures. The effective bandwidth becomes wider as the draft of the structures increases. The periodical length of the structures should be carefully chosen in practical applications. This study may provide informative guidance in the preliminary design of surface-piercing fixed structures based on the Bragg reflection to protect engineering structures or shoreline from wave attack.

Acknowledgements

The authors gratefully acknowledge the financial support from the Lloyd's Register Foundation (LRF) through the joint center involving University College London, Shanghai Jiao Tong University, and Harbin Engineering University. The LRF helps protect life and property by supporting engineering-related education, public engagement, and the application of research.

References

Bailard, J.A., DeVries, J.W., Kirby, J.T., Guza, R.T., 1990. Bragg reflection breakwater: a new shore protection method?. In: Proc. 22nd Int. Conf. on Coastal Eng., ASCE, N.Y., U.S, pp. 1702–1715.
Bailard, J.A., DeVries, J.W., Kirby, J.T., 1992. Considerations in using Bragg reflection for storm erosion protection. J. Waterw. Port, Coast. Ocean Eng. 118 (1), 62–74.
Chang, H.K., Liou, J.C., 2007. Long wave reflection from submerged trapezoidal breakwaters. Ocean Eng. 34 (1), 185–191.
Cho, Y.S., Lee, C., 2000. Resonant reflection of waves over sinusoidally varying topographies. J. Coast. Res. 16 (3), 870–876.
Cho, Y.S., Jeong, W.C., Woo, S.B., 2004. Finite element method for strong reflection of water waves. Ocean Eng. 31, 653–667.
Dalrymple, R.A., Kirby, J.T., 1986. Water waves over ripples. J. Waterw. Port, Coast. Ocean Eng. 112 (2), 309–319.
Ding, W.W., Zou, Z.J., Wu, J.P., 2018. Bragg reflection of water waves by multiple composite flexible membranes. Int. J. Offshore Polar Eng. 28 (02), 135–142.
Garnaud, X., Mei, C.C., 2010. Bragg scattering and wave-power extraction by an array of small buoys. Proc. R. Soc. London Ser. A-Math. Phys. Eng. Sci. 466 (2113), 79–106.
Hsu, T.W., Chang, H.K., Tsai, L.H., 2002. Bragg reflection of waves by different shapes of artificial bars. China Ocean Eng. 16 (3), 343–358.
Hsu, T.W., Tsai, L.H., Huang, Y.T., 2003. Bragg scattering of water waves by multiply composite artificial bars. Coast Eng. J. 45 (2), 235–253.
Jeon, C.H., Cho, Y.S., 2006. Bragg reflection of sinusoidal waves due to trapezoidal submerged breakwaters. Ocean Eng. 33, 2067–2082.
Karmakar, D., Bhattacharjee, J., Guedes Soares, C., 2013. Scattering of gravity waves by multiple surface-piercing floating membrane. Appl. Ocean Res. 39, 40–52.
Kar, P., Koley, S., Sahoo, T., 2018. Scattering of surface gravity waves over a pair of trenches. Appl. Math. Model. 62, 303–320.
Linton, C.M., 2011. Water waves over arrays of horizontal cylinders: band gaps and Bragg resonance. J. Fluid Mech. 670, 504–526.
Liu, P.L.-F., Abbaspour, M., 1982. An integral equation method for the diffraction of oblique waves by an infinite cylinder. Int. J. Numer. Methods Eng. 18, 1497–1504.
Liu, H.W., Luo, H., Zeng, H.D., 2014. Optimal collocation of three kinds of Bragg breakwaters for Bragg resonant reflection by long waves. J. Waterw. Port, Coast. Ocean Eng. 141 (3), 04014039.
Liu, H.W., Shi, Y.P., Cao, D.Q., 2015. Optimization of parabolic bars for maximum Bragg resonant reflection of long waves. J. Hydrodyn. 27 (3), 373–382.
Liu, Y., Li, H.J., Zhu, L., 2016. Bragg reflection of water waves by multiple submerged semi-circular breakwaters. Appl. Ocean Res. 56, 67–78.
Mei, C.C., Hara, T., Naciri, M., 1988. Note on Bragg scattering of water waves by parallel bars on the seabed. J. Fluid Mech. 186, 147–162.
Ouyang, H.T., Chen, K.H., Tsai, C.M., 2015. Investigation on Bragg reflection of surface water waves induced by a train of fixed floating pontoon breakwaters. Int. J. Nav. Archit. Ocean Eng. 7, 951–963.
Shih, R.S., Weng, W.K., 2016. Experimental determination of the performance characteristics of an undulating submerged obstacle. Ships Offshore Struct. 11 (2), 129–141.
Teng, B., Gou, Y., 2017. BEM for wave interaction with structures and low storage accelerated methods for large scale computation. J. Hydrodyn., Ser. B 29 (5), 748–762.
Tsai, L.H., Kuo, Y.S., Lan, Y.J., Hsu, T.W., Chen, W.J., 2011. Investigation of multiply composite artificial bars for Bragg scattering of water waves. Coast Eng. J. 53 (4), 521–548.
Tsai, L.H., Wen, C.C., 2010. Design of a series of submerged breakwaters for coastal protection against waves. China Ocean Eng. 24 (3), 553–564.
Wen, C.C., Tsai, L.H., 2008. Numerical simulation of Bragg reflection based on linear waves propagation over a series of rectangular seabed. China Ocean Eng. 22 (1), 71–86.
Zeng, H.D., Qin, B., Zhang, J.H., 2017. Optimal collocation of Bragg breakwaters with rectangular bars on sloping seabed for Bragg resonant reflection by long waves. Ocean Eng. 130, 156–165.